Sensing cooperativity in ATP hydrolysis for single multisubunit enzymes in solution

Yan Jiang[a,b], Nicholai R. Douglas[c], Nicholas R. Conley[a,1], Erik J. Miller[c,2], Judith Frydman[c], and W. E. Moerner[a,3]

[a]Department of Chemistry; [c]Department of Biology; and [b]Department of Applied Physics, Stanford University, Stanford, CA 94305

Contributed by W. E. Moerner, July 28, 2011 (sent for review June 21, 2011)

In order to operate in a coordinated fashion, multisubunit enzymes use cooperative interactions intrinsic to their enzymatic cycle, but this process remains poorly understood. Accordingly, ATP number distributions in various hydrolyzed states have been obtained for single copies of the mammalian double-ring multisubunit chaperonin TRiC/CCT in free solution using the emission from chaperonin-bound fluorescent nucleotides and closed-loop feedback trapping provided by an Anti-Brownian ELectrokinetic trap. Observations of the 16-subunit complexes as ADP molecules are dissociating shows a peak in the bound ADP number distribution at 8 ADP, whose height falls over time with little shift in the position of the peak, indicating a highly cooperative ADP release process which would be difficult to observe by ensemble-averaged methods. When AlFx is added to produce ATP hydrolysis transition state mimics (ADP·AlFx) locked to the complex, the peak at 8 nucleotides dominates for all but the lowest incubation concentrations. Although ensemble averages of the single-molecule data show agreement with standard cooperativity models, surprisingly, the observed number distributions depart from standard models, illustrating the value of these single-molecule observations in constraining the mechanism of cooperativity. While a complete alternative microscopic model cannot be defined at present, the addition of subunit-occupancy-dependent cooperativity in hydrolysis yields distributions consistent with the data.

single molecule | allostery | fluorescence | enzymology | nucleotide counting

Years of study of cooperativity for proteins with multiple ligand binding sites have yielded important insights, ever since the role of cooperative oxygen binding to hemoglobin in high oxygen-delivery throughput was recognized (1–3). Multisubunit enzymes usually hydrolyze ATP in a concerted fashion, but actually observing this process, enzyme by enzyme, can provide a deeper picture of the underlying cooperativity resulting from communication among the various subunits. A well known example has been the study of the rotary motor F1-ATPase by single-molecule techniques (4). Another class of multisubunit cellular machines is the double-ring type I and type II chaperonins which can have from 14 to 18 subunits each of which can hydrolyze ATP (5, 6). Ensemble studies of the bacterial type I GroEL/GroES system, for example, have indicated that ATP binds subunits in one 7-membered ring with positive cooperativity, while negative cooperativity operates between rings (7). We focus on the cooperative process operative in the mammalian type II chaperonin TRiC/CCT, which has two ring-shaped cavities with built-in lids composed of eight different subunits each. TRiC is essential for the folding of a number of key proteins in mammalian cells, including actin, tubulin, and many cell cycle regulators (8). Previous ensemble measurements of ATP-induced allosteric transition rates and steady-state ATPase rate in TRiC show evidence for positive and negative cooperativity during the ATPase cycle (9, 10). However, the molecular details of the cooperativity, such as which subunits are involved and whether the cooperativity in TRiC follows the same mechanism as other enzymes, have not been accessed so far by the conventional ensemble studies.

To explore these effects, we measure the stoichiometry of hydrolyzed ATP (in the form of either bound ADP or the transition state mimic, ADP·AlFx) in single TRiC enzymes and extract a new quantity, the hydrolyzed ATP number distribution, which may be interpreted as the probability of having a particular number of hydrolyzed ATP present on a single enzyme chosen at random. Knowing the shape of the full distribution from our single-molecule measurements goes beyond standard ensemble-averaged quantities and directly characterizes the native ATP-induced heterogeneity in TRiC chaperonins. In addition, the shape of the hydrolyzed ATP number distribution places strong bounds on models for the underlying cooperativity between the subunits, which enables us to rule out many standard models (11). While a complete microscopic model for the observed distributions would require additional future measurements, we show by example that addition of subunit-occupancy-dependent hydrolysis to conventional cooperativity analysis yields distributions consistent with the data.

Optical studies of single biological molecules in solution face a major challenge: Due to rapid Brownian motion, individual molecules can only stay in the laser focal volume for a few milliseconds, limiting the information obtained. Surface immobilization, which can extend the observation time, may introduce disturbances to the function of the molecules (12, 13) or even may require cross-linking of multisubunit complexes to prevent surface-induced degradation (14). To address this problem, a device termed the Anti-Brownian ELectrokinetic trap (ABEL trap) has been developed as a noncontacting approach for extending the observation time of single fluorescent biomolecules in free solution (15). Among other advantages, the ABEL trap is optimized for a certain size of diffusing object (here ~1 MDa TRiC) so tiny unbound single fluorophores are not trapped, thus providing better differentiation between the target protein and any free fluorophores compared to surface immobilization methods. In our experiment, TRiC chaperonins are trapped individually by the ABEL trap and the numbers of fluorescent ATP hydrolyzed (in one cycle) and still attached to each enzyme are counted to build up a distribution of nucleotide numbers as described below.

The ABEL trap localizes a fluorescent particle by measuring the position of the particle in real time and actively applying feedback forces to counteract Brownian displacements and thus maintain the particle near the center of the trap. The trap detects the two-dimensional location of a fluorescent object with a hardware-based rotating beam scheme originally proposed by Enderlein (16) and implemented by Berglund and Mabuchi (17, 18) for particle tracking, as opposed to trapping. The center of the trap is illuminated by a focused pump laser beam revolving in

Author contributions: Y.J., J.F., and W.E.M. designed research; Y.J. and N.R.D. performed research; Y.J., N.R.D., N.R.C., and E.J.M. contributed new reagents/analytic tools; Y.J. analyzed data; and Y.J., J.F., and W.E.M. wrote the paper.

The authors declare no conflict of interest.

See Commentary on page 16865.

[1]Present address: Department of Radiology, Stanford University, CA 94305.

[2]Present address: Pacific Biosciences, Menlo Park, CA 94025.

[3]To whom correspondence should be addressed. E-mail: wmoerner@stanford.edu.

This article contains supporting information online at www.pnas.org/lookup/suppl/doi:10.1073/pnas.1112244108/-/DCSupplemental.

www.pnas.org/cgi/doi/10.1073/pnas.1112244108

a circular pattern at 40 kHz; an off-center particle emits fluorescence that is modulated at the same rate. The phase of this modulation can be used to determine in which direction the particle has moved from the trap center in the $x-y$ plane. Then the required feedback force is generated by applying voltages to the solution in a microfluidic geometry (see Fig. 1*A*) to move the particle back to the center by electro-osmotic forces. The detection and feedback occur continuously so that the particle is localized in a small region of uniform optical intensity at the center of the trap for times on the order of seconds. Meanwhile the third (z) dimension of motion is restricted by the top and bottom walls of a 750 nm thick quartz microfluidic channel. For full details of the ABEL trap design, see ref. 19, *Methods*, and *SI Text*.

In order to count the number of ATP molecules hydrolyzed by each chaperonin, every ATP molecule is covalently labeled with a Cy3 fluorophore (*SI Appendix: Fig. S2 and S3*). Two kinds of samples were prepared for study. The first type of sample consists of TRiC/Cy3-ADP complexes designed to allow observation of the time-dependent ADP release process in the ABEL trap. This sample is formed by incubating TRiC with 200 μM Cy3-ATP for 45 min, sufficient time to reach steady state. After removal of unbound nucleotides by size-exclusion purification (which defines $t = 0$), roughly 10 min are required to load the TRiC/Cy3-ADP complexes into the microfluidic cell of the ABEL trap. Green 532 nm excitation light pumps the Cy3-ADP molecules still bound to TRiC (Fig. 1*A* inset) thus generating the fluorescence signal needed for trap operation, that is, only TRiC with fluorescent nucleotides bound are trapped. When a fluorescent TRiC molecule diffuses into the trap, the trap forces hold the complex in a region of uniform pumping intensity for an extended period on the order of 1 s (Fig. 1*B*). At the same time, the continuous irradiation produces stepwise decreasing fluorescence intensity traces, which reflect the photobleaching of individual Cy3 dyes (Fig. 1*C*). The number of these steps and, therefore, the number of fluorescent ADP molecules on each chaperonin can then be determined (although in practice the number of Cy3-ADP is more reliably determined by the initial brightness divided by the average brightness for one Cy3, see *SI Appendix: Fig. S6*). Because any released Cy3-ADP is far smaller than TRiC and diffuses away rapidly, trapping experiments on this sample only sense TRiC enzymes with Cy3-ADP which has not yet dissociated from the enzyme. As a result, the number distribution of the Cy3-ADP still bound to the chaperonin can change over time due to the release of Cy3-ADP into the solution.

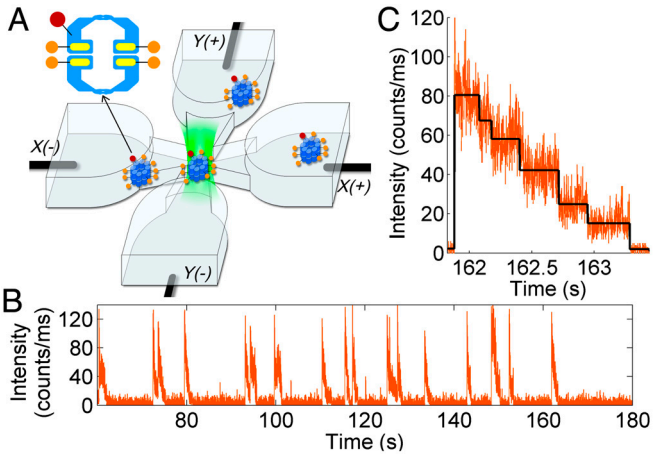

Fig. 1. Experimental design and example data. (*A*) Schematic of experiment showing the microfluidic channels of the ABEL trap. Each blue object signifies a single closed Atto647-TRiC molecule with several Cy3-labeled nucleotides bound. Inset: Blue structure: TRiC molecule with both cavities closed; Red dot: Atto647 dye; Orange dots: Cy3 dyes bound to ADP molecules (yellow bars). (*B*) Fluorescence signal from Cy3 showing individual trapped TRiC with several bound nucleotides entering the trap and photobleaching. (*C*) Expansion of the time axis for one of the events. The black line depicts the steps found by the change-point-finding algorithm reflecting the photobleaching of individual Cy3 dyes.

In order to obtain insight from different ATP incubation concentrations, remove the time-dependence, and additionally detect TRiC molecules with no nucleotide, a second type of sample was prepared where each chaperonin is also surface-labeled with a red Atto647 fluorophore (*SI Appendix*). Furthermore, AlFx, a phosphate analog that binds to hydrolyzed ATP after P_i release to form the transition state mimic ADP·AlFx (20), was included in the 45 min incubation of Atto647-TRiC with Cy3-ATP to form stable Atto647-TRiC/Cy3-ADP·AlFx complexes. These complexes have the hydrolysis cycle arrested at the transition state, a state which has previously been characterized as the closed form of the chaperonin (21). Because these chaperonins represent ADP·AlFx bound forms after the departure of inorganic phosphate, they are used to count the number of ATP molecules hydrolyzed by each TRiC in steady state. These complexes are stable for an extended period (hours), allowing removal of unbound nucleotides and loading into the microfluidic cell to measure the full ADP·AlFx number distribution. In a separate measurement pumping the Atto647 label with 638 nm light, the total number of TRiC entering the trap volume in a fixed time is determined, whether or not Cy3-ADP·AlFx molecules are bound. Distributions of the number of Cy3-ADP·AlFx molecules present on each stable complex are obtained in this way for incubation Cy3-ATP concentrations from 5 μM to 1.5 mM.

Results

Counting ADP on TRiC/Cy3-ADP Complexes as Function of Time. In the TRiC/Cy3-ADP samples without AlFx, the Cy3-ADP is not locked to TRiC, which allows us to indirectly observe the process of TRiC releasing ADP. In principle, incubation of TRiC with Cy3-ATP for 45 min, followed by purification of nucleotide-containing chaperonin complexes could yield a TRiC with both Cy3-ATP and Cy3-ADP bound. However, at least 10 min elapsed in the experiments before the purified complexes could be loaded into the trap; given the rate of ATP hydrolysis by TRiC (0.75 ± 0.07 M ATP/M TRiC/min for $[\mathrm{ATP}] = 200$ μM at room temperature, *SI Appendix: Fig. S5*), it is reasonable to expect that only TRiC with ADP waiting to dissociate would be observed. Because any released Cy3-ADP diffuses much faster than TRiC/Cy3-ADP complexes and therefore is not trapped, then for each trapped single TRiC/Cy3-ADP complex, the fluorescence emission is analyzed to obtain the number of nucleotides bound to each TRiC. A change-point finding algorithm of Watkins, et al. (22, 23) is used to resolve the photobleaching steps in the intensity traces (Fig. 1*B*) and extract an average brightness for a single Cy3. Then the number of Cy3-ADP and its estimated measurement uncertainty are calculated for each chaperonin and the results are used to generate a unique type of ADP number (N_{ADP}) distribution which includes information about the counting uncertainty (see *SI Appendix: Fig. S6* for details). The resulting ADP number distribution is displayed in several ways (Fig. 2*A* shows an example distribution for the 10–15 min period measured from the end of the size-exclusion purification step): (*i*) as a simple histogram of integer ADP numbers using the gray histogram bars in the background, (*ii*) as a set of colored continuous curves which reflect the uncertainty in the determination for each N_{ADP}, and (*iii*) as the red curve which is the resulting overall distribution. A small fraction of TRiC molecules seemed to show $N_{\mathrm{ADP}} = 1$, 2, or 3, but because such peaks also occurred in pure buffer (*SI Appendix: Fig. S10*) at the same frequency as in the samples prepared at different incubation ATP concentrations, with or without AlFx (*SI Appendix: Table S1*), these peaks were attributed to impurities and are not shown in Fig. 2.

Fig. 2*B* shows the observed ADP number distributions, where only the full distributions are displayed at various time points. The size of the distribution peak understandably decreases over time

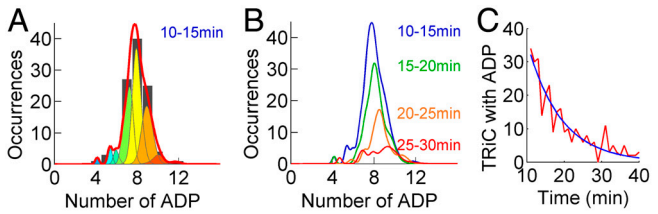

Fig. 2. Measured ADP number distributions during time-dependent ADP release. Enzymes were incubated with 200 μM Cy3-ATP for 45 min followed by removal of free nucleotide, which defines $t = 0$. (*A*) The ADP number distribution for single enzymes in the ABEL trap between 10 and 15 min. The gray histogram bars in the background are the integer-rounded ADP numbers for every complex. The colored areas are the continuous distributions of the actual ADP numbers for the complexes grouped in each gray bar. The red curve is the sum of all the distributions and is therefore the full distribution. The data for ADP numbers 1–3 arising mostly from impurities are not shown (*SI Appendix: Fig. S7*). (*B*) As Cy3-ADP is released from TRiC, the ADP number distribution varies with time. (*C*) The ensemble-averaged number of TRiC with ≥1 ADP as a function of time (red data) can be fit to a single exponential decay (blue curve).

due to the continuing release of the Cy3-ADP, but the abscissa of the peak remains large, near eight nucleotides (Fig. 2*B*). The constancy of the peak position during the ADP release process reveals that the process is highly cooperative, otherwise complexes with 5, 4, etc. nucleotides would have been observed. By integrating these distributions, the number of detected TRiC with any number of Cy3-ADP bound as a function of time can be fit with a single exponential decay as shown in Fig. 3*B*. This result implies that TRiC/Cy3-ADP likely changes conformation to a low affinity state with a simple first-order reaction rate constant (0.11 ± 0.03/ min as fitted) and then rapidly releases all the ADP. Given that each TRiC hydrolyzes about eight ATP molecules at one time, the observed ADP release rate is 0.88 ± 0.22/chaperonin/ min. This rate is comparable to the steady-state ATP hydrolysis rate measured separately in ensemble experiments under the same conditions (0.75 ± 0.07 M ATP/M TRiC/min, *SI Appendix: Fig. S5*).

Counting ATP Transition State Mimics Using Stable Atto647-TRiC/Cy3-ADP·AlFx Complexes. In addition to observation of time-dependent ADP release, stable single Atto647-TRiC/Cy3-ADP·AlFx complexes are trapped to obtain the ADP·AlFx number ($N_{\text{ADP·AlFx}}$) distributions at various incubation ATP concentrations ([ATP]). Fig. 3 shows six representative $N_{\text{ADP·AlFx}}$ distributions at [ATP] = 5 μM, 10 μM, 25 μM, 50 μM, 200 μM, and 1 mM. First, as one

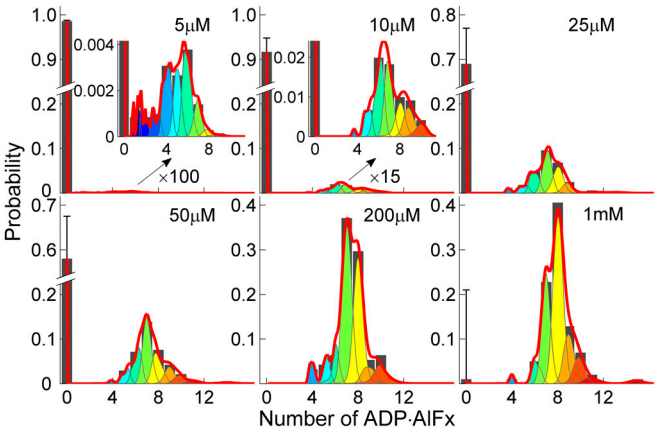

Fig. 3. ADP·AlFx number distributions for single TRiC complexes at six different incubation ATP concentrations. The distributions are displayed as in Fig. 2 except normalized by the total number of TRiC into probability distributions. The error bar (the symmetric lower half is not shown) is the uncertainty of the measured probability of TRiC with no ADP·AlFx. Insets: Expansion of the distributions at [ATP] = 5 μM and 10 μM. For [ATP] > 5 μM, the spurious peaks at ADP·AlFx numbers 1–3 (*SI Appendix: Fig. S8*) are not shown as in Fig. 2.

would expect, the fraction of TRiC with zero ADP·AlFx is large at low [ATP], and this fraction drops quickly to zero at high incubation concentration. As in Fig. 2, the spurious peaks at $N_{\text{ADP·AlFx}} = 1$, 2, or 3 are not shown except at [ATP] = 5 μM. The primary characteristics of the $N_{\text{ADP·AlFx}}$ distributions in Fig. 3 are the predominant single peak for all ATP incubation concentrations and the fact that $N_{\text{ADP·AlFx}}$ jumps very quickly to large values. For [ATP] ≥ 25 μM, the center of the peak is always between 7 and 8 and the height of the peak increases as [ATP] increases. Only when [ATP] < 25 μM does the center of the peak move to smaller numbers like 6 or 5, even though the fraction of TRiC containing ADP·AlFx is only 1.5% of the total TRiC. At [ATP] > 200 μM, essentially all TRiC contain 7 or 8 ADP·AlFx. No other peaks show up even when [ATP] is as high as 1.5 mM (*SI Appendix: Fig. S9*), a concentration which saturates the TRiC ATPase activity (10). Analyzing the shape of the average number of ADP·AlFx per TRiC vs. [ATP], the apparent Hill coefficient is calculated to be 1.6 ± 0.6, which suggests positive cooperativity in TRiC (*SI Appendix: Fig. S11*).

These single-molecule counting data provide the surprising suggestion that for most incubation concentrations, only seven or eight ATP are hydrolyzed at one time in each 16-subunit TRiC complex. It would be useful to know whether all eight occupy one of the rings with the other ring empty or if the hydrolyzed ATP distribute over both rings. Because the transition state of ATP hydrolysis is known to induce the closure of both TRiC cavities (21), to answer the above question, a proteinase *K* digestion assay was employed which clips off the lid domains of TRiC for any cavity that is not closed. For [ATP] ≥ 1 mM, over 85% of the TRiC molecules are fully protected against the proteinase *K* digestion, i.e., both rings are closed (*SI Appendix: Fig. S4*). Combining this information with the ADP·AlFx counting experiments at the same ATP concentrations, we conclude that the TRiC molecules with $N_{\text{ADP·AlFx}} = 8$ are likely to be in the symmetric both-cavity-closed conformation. The symmetry of the both-cavity-closed conformation implies that a TRiC molecule most likely hydrolyzes four ATP in each ring (a conclusion also consistent with a separate cross-linking study, *vide infra*). The fact that not all the 16 subunits hydrolyze ATP can be a consequence of heterogeneous binding affinities of the different subunits or negative cooperativity between the subunits or a combination of both mechanisms, which will be considered below.

Discussion

The ADP number distributions directly show the time-dependence of the nucleotide release process (Fig. 2) and the fractions of various TRiC/ADP·AlFx species which are present for specific incubation concentrations (Fig. 3), measurements which extend beyond conventional ensemble-averaged approaches and which have not been available previously. Therefore, it is useful to examine which types of cooperativity models might give rise to the observed behavior, and we do this for Fig. 2 briefly first and then in detail for Fig. 3. Surprisingly, the data reveal shortcomings

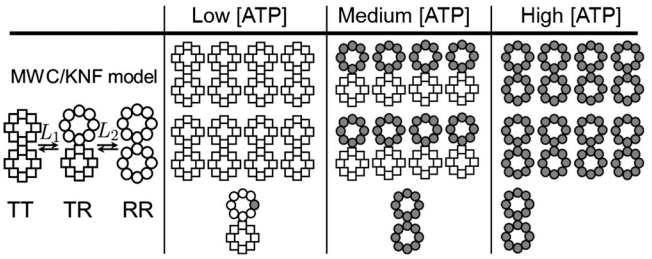

Fig. 4. Illustration of a conventional MWC/KNF cooperative ATP binding model and the corresponding composition of TRiC populations for various ATP concentration regimes. The squares and circles signify subunits of TRiC in tense/relaxed states, respectively, with filled shapes signifying subunits with ATP bound. L_1 and L_2 are cooperativity equilibria.

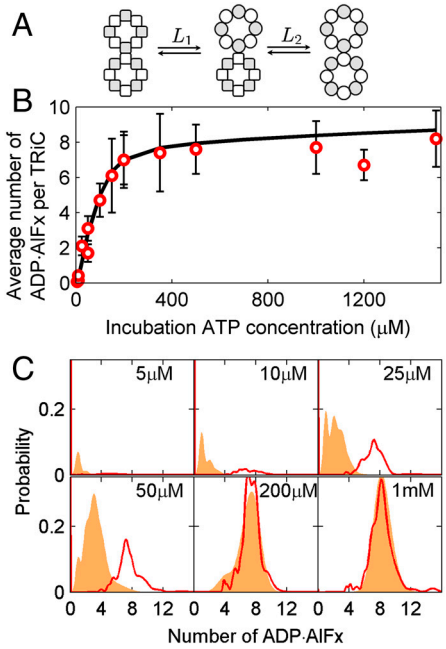

Fig. 5. First trial model and its prediction. (*A*) Scheme for the first trial model. The squares and circles signify subunits of TRiC in tense/relaxed states, respectively; white shapes have higher ATP binding affinity than gray ones. (*B*) Comparison between model and experiment for ensemble data. Circles: experimental data; solid curve: calculated from the model. (*C*) Comparison between model and experiment for single-molecule data. The orange areas show the ADP·AlFx number distributions calculated from the model, which are broadened by an amount effectively equal to one nucleotide to approximate the counting uncertainty in experimental measurement. The experimental data of Fig. 3 are shown in the red curves.

of standard cooperativity models in that the predicted $N_{\text{ADP·AlFx}}$ distributions from conventional models depart significantly from the data. To go further, recognizing that the eight subunits in each ring are not identical, we have created two trial models in which previously measured subunit-dependent binding heterogeneity is added to conventional cooperativity, but these two models also do not fit the data. It is not unusual that when unique data become available, that the microscopic mechanisms giving rise to the new behavior are not fully understood for some time. Nevertheless, we conclude by providing a putative model which includes subunit-occupancy-dependent cooperativity in hydrolysis and which mimics the data well. Even though this is not intended to be a final microscopic picture, our proof-of-principle demonstration that some model can fit the observed data should help stimulate future work to understand the observed behavior.

Cooperativity in ADP Release. Fig. 2 clearly shows strong cooperativity in ADP release process, which has not been observed previously. The exponential shrinking of the single peak at eight in the ADP number distribution indicates a conversion between two distinct TRiC populations, one with eight ADP and one empty. This conversion can be modeled with a conventional Monod-Wyman-Changeux (2) style cooperativity, in which all the subunits in TRiC simultaneously change conformation between high and low ADP affinity:

$$\text{TRiC(high affinity)} \cdot \text{ADP} \overset{L}{\leftrightarrow} \text{TRiC(low affinity)} \cdot \text{ADP},$$

with L the equilibrium constant. Once an enzyme enters the low affinity state, it quickly releases all the ADP on it. Therefore the low affinity population is always observed as devoid of nucleotide, is nonfluorescent, and is not detected in the experiments. The agreement between the ADP release rate measured by the ABEL trap experiment and the steady-state ATP hydrolysis rate measured by biochemical assay implies that ADP release is the rate limiting step in the ATPase cycle as is common in many enzymes. Given that TRiC has both cavities closed when incubated with 200 μM ATP (10), this long-lasting ADP bound state (~6 min half life) must have both cavities closed as well. Therefore the slow decay of the high ADP affinity state apparently represents the timer for the ATPase cycle and may be present to allow a sufficient amount of time for any enclosed polypeptide substrate to attempt to reach the folded state.

Standard Cooperativity Models. In addition to the time-dependent ADP release, the ADP·AlFx number distributions at various incubation ATP concentrations (Fig. 3) also show strong evidence of cooperativity between TRiC subunits in multiple ways: the existence of primarily two distinct populations, the empty TRiC, and the eight-nucleotide-bound TRiC; the rapid accumulation of the eight-nucleotide-bound TRiC as [ATP] increases; and the larger-than-one Hill coefficient. Because AlFx locks ADP on TRiC after ATP binds and becomes hydrolyzed, we first consider cooperative binding with the well known models for cooperative ligand binding (11, 24) in multisubunit proteins and enzymes, including the Monod-Wyman-Changeux (MWC) model (2) and the Koshland-Nemethy-Filmer (KNF) model (3). Originally developed to explain cooperative oxygen binding in hemoglobin, these models have also been applied to previous ensemble experiments of ATP binding in chaperonins. For example, in a transient kinetic study, Horovitz and coworkers (9) measured the rates of appearance of ATP-induced conformational changes in TRiC at different [ATP] and obtained a bisigmoidal curve indicating positive cooperativity at low [ATP] and negative cooperativity at intermediate [ATP]. The authors were able to fit their data by modeling the positive cooperativity with the MWC model and the negative cooperativity with the KNF model. By no accident, the ensemble-averaged cooperativity behavior we measure, computed from the average number of ADP·AlFx vs. [ATP], can also be fit with combinations of MWC and KNF models and appropriate subunit binding affinities as will be discussed below (Fig. 5*B*, *SI Appendix: Fig. S11*B). However, as will be demonstrated presently, the single-molecule $N_{\text{ADP·AlFx}}$ distributions

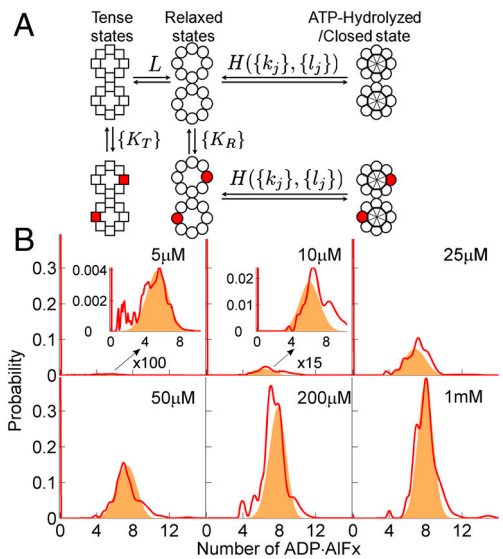

Fig. 6. Subunit-occupancy-dependent model and its prediction. (*A*) Illustration of the model. The squares and circles signify subunits of TRiC in tense/relaxed states, respectively, with red signifying subunits with ATP or ADP·AlFx bound. K's represent binding equilibria, L's cooperativity equilibria, H's hydrolysis probabilities (*SI Appendix*). For the specific case shown where only subunit CCT5 has ATP bound in both rings, the hydrolysis probability is $H(\{0,0,0,0,1,0,0,0\},\{0,0,0,0,0,1,0,0\})$. (*B*) Comparison between model and experiment, displayed in the same way as Fig. 5*C*.

in Fig. 3 cannot be explained by simple combinations of these cooperative binding models alone.

First we consider the standard model combining MWC and KNF, which is used for describing the cooperativity in ATPase activity of GroEL (7, 9). Here we are making the assumption that the binding process dominates what is observed in terms of ADP·AlFx numbers after ATP hydrolysis (Fig. 3), i.e., all complexes with specific numbers of ATP bound proceed to hydrolysis with equal probability. Each of the sixteen subunits in TRiC can be in either the tense (T) state (low affinity for ATP) or the relaxed (R) state (high affinity to ATP). The eight subunits within each ring of TRiC obey MWC, i.e., all the eight subunits change conformation simultaneously; whereas the two rings follow KNF, i.e., they change conformation in a sequential fashion. Based on these assumptions, there exists three states for each TRiC: both rings tense (TT), one ring tense and one ring relaxed (TR), and both rings relaxed (RR), between which there are two equilibrium constants L_1 and L_2, also called allosteric constants (Fig. 4). In the absence of ATP, the equilibrium distribution consists of a majority of TT molecules and only a tiny portion of TR and RR molecules. As ATP is introduced to the solution, the TR molecules quickly bind ATP and more molecules transform into the TR state in order to maintain the equilibrium. As a result, as soon as [ATP] exceeds a certain concentration C_1, the dominant TT population rapidly converts to a dominant TR population. Similarly, as the ATP concentration further increases above another critical concentration C_2, the RR molecules dominate. In the language of the ATP number distributions, these conversions correspond to a quick transition between a single peak at zero ATP to a single peak at eight around the concentration C_1 and another quick transition between a single peak at eight to a single peak at sixteen around the concentration C_2, which is characteristic of positive cooperativity. On the other hand, in between C_1 and C_2, increasing [ATP] results in little change in the ATP number distribution, which is recognized as negative cooperativity. Comparing to the observed $N_{\mathrm{ADP\cdot AlFx}}$ distributions in Fig. 3, which never reach sixteen, this model is not readily applicable to our data.

Standard Cooperativity Models Including Subunit-Dependent Binding Affinity. To probe further, we searched for modifications of MWC/KNF which would predict bound ATP number distributions with a single peak at eight for saturating ATP concentration, again assuming $N_{\mathrm{ADP\cdot AlFx}}$ follows the bound ATP number. Fortunately, a previous study by Reissmann [published online (26)] provides a rational direction for modification. In this study, the researcher crosslinked azide-labeled radioactive ATP to TRiC using UV-induced photoaffinity labeling; then the TRiC subunits were separated and analyzed by HPLC; finally scintillation counting was used to measure the presence of ATP in each eluted TRiC subunit fraction. This cross-linking study found that only four of the eight different subunits in each ring have ATP bound at saturating [ATP], indicating only four of them have high affinity to ATP. Using this heterogeneity in ATP binding affinities, we generated two trial MWC-and-KNF-based cooperativity models that might allow us to observe a major population of TRiC with four ATPs hydrolyzed in each ring assuming all complexes with specific numbers of ATP bound proceed to hydrolysis with equal probability. Using a probabilistic analysis of the various possibilities for ATP binding (*SI Appendix*), the predicted theoretical $N_{\mathrm{ADP\cdot AlFx}}$ distributions were calculated at each incubation ATP concentration to be compared with the experimental distributions. Even though these modifications represent improvements, intrinsic discrepancies still occur between each of the candidate models and the experimental data, therefore only one of the models will be summarized here (see *SI Appendix* for details of both models).

For trial model I, positive cooperativity is assumed between the eight subunits within one ring of TRiC, simulated by MWC, and negative cooperativity is assumed between the two rings, simulated by KNF; while only four of the eight dissociation constants K_R for the relaxed state subunits are lower than the saturating ATP concentration (Fig. 5*A*). Fig. 5*B* presents the ensemble-averaged $N_{\mathrm{ADP\cdot AlFx}}$ per TRiC calculated from our measurements in Fig. 3 and from the model to show that ensemble-averaged data do not show a discrepancy, but the single-molecule distributions (red curves in Fig. 5*C*) do show a significant departure from the predicted $N_{\mathrm{ADP\cdot AlFx}}$ distributions (orange in Fig. 5*C*).

Similar to trial model I, another trial model which makes different assumptions about positive and negative cooperativity also matches the ensemble-averaged data but departs significantly from the single-molecule data at [ATP] < 200 μM (*SI Appendix: Fig. S12*). We certainly cannot exhaust all the possible combinations of the classic models. However, any allosteric binding model would share the same failure as the above models do in mimicking the distributions at low [ATP]. For example, these models cannot produce a single peak centered at 5 which represents as small as 1.5% of the total population yet does not grow into 100% of the total population until [ATP] increases by 40 times (refer to *SI Appendix* for more details). Thus there must be more complex cooperative interactions between TRiC subunits.

Subunit-Occupancy-Dependent Cooperativity. Up to this point, we have included subunit-dependent binding affinity, but assume that no further interactions occur between the subunits as the hydrolysis proceeds. Of course, the residues along the boundaries of the subunits of TRiC would naturally be expected to be able to provide a means for intersubunit communication in hydrolysis as well as in binding. It is also true that our measurements in Fig. 3 do not specifically measure the binding configuration itself before hydrolysis, rather we only sense the nucleotides that became hydrolyzed and locked onto the enzyme. Therefore, it will not be possible to deduce a unique microscopic model from the data as more than one cooperative process may be involved. Nevertheless, it is valuable to show at least one putative model which can mimic the observations better than the models already described. As mentioned above, compared to the above models, the experimental data shows a striking preference for TRiC to have eight ADP·AlFx locked on each complex *relatively independent of the ATP concentration*, thus we add a subunit-occupancy-dependent function to include this preference.

Our proof-of-principle model consists of two parts, ATP binding and ATP hydrolysis. The ATP binding process is modeled with MWC with Hill coefficient h ~ 1, which gives neither positive nor negative cooperativity. This neutral setting is chosen for simplicity because the exact Hill coefficient of the ATP binding process alone is unknown. If the binding process has a different Hill coefficient, the parameters of the subunit-occupancy-dependent cooperativity model would need to be adjusted accordingly. In addition, using the evidence from the cross-linking experiment [Reissmann, published online (26)] that only four subunits in each ring have high binding affinities that allow ATP to bind at saturating ATP concentration, four of the eight different subunits are constrained to have larger association constants than the others. Finally the hydrolysis probability of the ATP-bound TRiC is assumed to be a function of the specific ATP-occupied subunits (Fig. 6*A*). Depending on the functional behavior of the hydrolysis probability vs. the number of bound ATPs, binding more ATP can either promote or prohibit hydrolysis, which will yield the required positive or negative cooperativity. For example, one specific hypothesis that would create a trend in the hydrolysis probability which matches our data is this: when ATP is bound to the high affinity subunits CCT5, CCT1, CCT2, and CCT4, this grouping actively assists the conformational change proceeding to hydrolysis while binding to the other four subunits prevents the hydrolysis. Because the high affinity subunits are more likely to bind ATP, having more ATP bound first promotes the hydrolysis but very soon when additional ATP molecules bind to the low

affinity subunits CCT7, CCT8, CCT3, and CTT6, the ability to hydrolyze ATP in the complex is prohibited. As a result, TRiC molecules with four ATP bound in each ring are most favored to proceed to the hydrolyzed form.

Mathematically, this hypothesized behavior can be provided by the following equilibrium equation for the concerted hydrolysis (written as concentration ratio between open and closed TRiC),

$$\frac{[\text{closed TRiC}(\{k_j\};\{l_j\})]}{[\text{open TRiC}(\{k_j\};\{l_j\})]} = H(\{k_j\};\{l_j\}) = H_0 \times \alpha^{\Sigma_{j=1,2,4,5}(k_j+l_j)} \times \beta^{\Sigma_{j=3,6,7,8}(k_j+l_j)}.$$

Where H is the hydrolysis probability function which depends upon the specific ATP occupancy vectors given by $\{k_j\}$ and $\{l_j\}$, two sets of eight numbers with values 0 and 1, a binary indicator denoting whether each subunit is occupied by ATP in each ring, H_0 is the base hydrolysis probability for TRiC with no ATP bound, and α and β are dimensionless parameters ($\alpha > 1$, $0 < \beta < 1$). The hydrolysis probability for each ATP binding configuration in TRiC can therefore be calculated. For example, the hydrolysis probability for a TRiC molecule with ATP bound in the CCT5, 1, 2, and 4 subunits of both rings is $H(\{10110010\};\{10110010\}) = H_0 \times \alpha^8 \times \beta^0$. Given these assumptions, the exact population of each TRiC conformation with various numbers of bound ATP can be computed to build the expected ADP·AlFx number distribution. The precise details of the model, including the fitting parameters, are described in the *SI Appendix*. As shown in Fig. 6*B*, the calculated probability distributions for $N_{\text{ADP·AlFx}}$ (orange) mimic the shape of the measured $N_{\text{ADP·AlFx}}$ distributions (red curves) very well. Thus subunit-occupancy-dependent cooperativity can be a plausible explanation for our observations.

The exact cause of this subunit-occupancy-dependent cooperativity could arise from a number of microscopic interactions defined by contacts between neighboring subunits. For example, the inter-/intraring contact between a high affinity and a low affinity subunit might inhibit simultaneous hydrolysis in both subunits. Without additional measurements of the critical local interactions, here we have simply analyzed the consequence but not the mechanism of this cooperativity. Even though our putative model certainly may not be the only way to achieve the proper cooperative behavior, it does represent a proof-of-principle that a plausible model can be developed which includes only three additional parameters. In future studies, more complex (and more physical) models can then be generated which would directly capture the ways in which the subunit conformations driven by the presence of ATP influence the ability of neighboring subunits to bind and/or hydrolyze ATP.

Conclusion

In these experiments, the ABEL trap has been used to study the single-molecule stoichiometry of ADP and the ATP transition state mimic ADP·AlFx for the multisubunit enzyme TRiC in free aqueous solution. The distributions of nucleotide number on individual TRiC complexes show that TRiC either hydrolyzes no ATP or hydrolyzes about four ATP in each of the two rings at the same time over an ATP incubation concentration range from 25 μM to 1.5 mM. In addition, the ADP release process is found to be highly cooperative by directly observing ADP number distributions as a function of time. Because the ADP·AlFx number distributions extracted from single-molecule data place strong constraints which allow a number of simple models to be excluded, we postulate the existence of subunit-occupancy-dependent cooperativity, which can only be conclusively proven in future studies. With the powerful capability provided by ABEL trap measurements of single molecules in solution, the nucleotide or substrate stoichiometry in other multisubunit enzymes can be directly measured with maximum preservation of the native activities and used to constrain our understanding of enzymatic mechanisms.

Methods

The *SI Appendix* contains full details of data analysis, modeling, labeling, biochemical measurements, and description of controls. All errors are reported as standard error of the mean.

Briefly, the ABEL trap optical setup resembles a typical confocal fluorescence microscope except that a 532 nm excitation laser beam is deflected by a pair of acoustooptic deflectors before entering the microscope so that the laser focus revolves in a circle in the sample plane at 40 kHz to yield a time averaged spatially uniform optical intensity over a disk. The modulated fluorescence photons from a TRiC molecule containing bound fluorescent nucleotides are collected by an avalanche photodiode and the phase of the modulation is analyzed by bespoke phase sensing electronics to obtain the direction of displacement of the fluorescent object from the trap center. The circuit then applies correct feedback voltages on four electrodes in the microfluidic cell to drift the object back to the center of the laser rotation (19, 25).

ACKNOWLEDGMENTS. The authors thank Randall Goldsmith for experimental assistance and useful discussions and Adam E. Cohen and Stefanie Reissmann for crucial assistance in the initial phase of this project. This work was supported in part by Award No. PN2-EY016525 from the National Eye Institute of the National Institutes of Health and by a Larry Yung Stanford Graduate Fellowship to Y.J.

1. Adair GS, Bock AV, Field HJ (1925) The hemoglobin system: VI. The oxygen dissociation curve of hemoglobin. *J Biol Chem* 63:529–545.
2. Monod J, Wyman J, Changeux JP (1965) On the nature of allosteric transitions: a plausible model. *J Mol Biol* 12:88–118.
3. Koshland DEJ, Némethy G, Filme D (1966) Comparison of experimental binding data and theoretical models in proteins containing subunits. *Biochemistry* 5:365–385.
4. Kinosita K, Jr, Adachi K, Itoh H (2004) Rotation of F1-ATPase: how an ATP-driven molecular machine may work. *Annu Rev Biophys Biomol Struct* 33:245–268.
5. Klumppa M, Baumeister W (1998) The thermosome: archetype of group II chaperonins. *FEBS Lett* 430:73–77.
6. Braig K, et al. (1994) The crystal structure of the bacterial chaperonin GroEL at 2.8 A. *Nature* 371:578–586.
7. Yifrach O, Horovitz A (1995) Nested cooperativity in the ATPase activity of the oligomeric chaperonin GroEL. *Biochemistry* 34:5303–5308.
8. Frydman J (2001) Folding of newly translated proteins in vivo: the role of molecular chaperones. *Annu Rev Biochem* 70:603–647.
9. Kafri G, Horovitz A (2003) Transient kinetic analysis of ATP-induced allosteric transitions in the eukaryotic chaperonin containing TCP-1. *J Mol Biol* 326:981–987.
10. Reissmann S, Parnot C, Booth CR, Chiu W, Frydman J (2007) Essential function of the built-in lid in the allosteric regulation of eukaryotic and archaeal chaperonins. *Nat Struct Mol Biol* 14:432–440.
11. Fersht A (1999) *Structure and Mechanism in Protein Science* (Freeman, New York) p 631.
12. Goldstein L (1976) Kinetic behavior of immobilized enzyme systems. *Method Enzymol* 44:397–443.
13. Friedel M, Baumketner A, Shea JE (2006) Effects of surface tethering on protein folding mechanisms. *Proc Natl Acad Sci USA* 103:8396–8401.
14. Shin Y, et al. (2009) Single-molecule denaturation and degradation of proteins by the AAA+ ClpXP protease. *Proc Nat Acad Sci USA* 106:19340–19345.
15. Cohen AE, Moerner WE (2006) Suppressing Brownian motion of individual biomolecules in solution. *Proc Natl Acad Sci USA* 103:4362–4365.
16. Enderlein J (2000) Tracking of fluorescent molecules diffusing within membranes. *Appl Phys B* 71:773–777.
17. Berglund AJ, Mabuchi H (2004) Feedback controller design for tracking a single fluorescent molecule. *Appl Phys B* 78:653–659.
18. Berglund AJ, Mabuchi H (2005) Tracking-FCS: fluorescence correlation spectroscopy of individual particles. *Opt Express* 13:8069–8082.
19. Cohen AE, Moerner WE (2008) Controlling Brownian motion of single protein molecules and single fluorophores in aqueous buffer. *Opt Express* 16:6941–6956.
20. Chabre M (1990) Aluminofluoride and beryllofluoride complexes: new phosphate analogs in enzymology. *Trends Biochem Sci* 15:6–10.
21. Meyer AS, et al. (2003) Closing the folding chamber of the eukaryotic chaperonin requires the transition state of ATP hydrolysis. *Cell* 113:369–381.
22. Watkins LP, Yang H (2005) Detection of intensity change points in time-resolved single-molecule measurements. *J Phys Chem B* 109:617–628.
23. Boudjellaba H, MacGibbon B, Sawyer P (2001) On exact inference for change in a Poisson sequence. *Commun Stat-Theory M* 407–434.
24. Ferrell JEJ (2009) Q&A: cooperativity. *Journal of Biology* 8:53.
25. Goldsmith RH, Moerner WE (2010) Watching conformational- and photodynamics of single fluorescent proteins in solution. *Nature Chemistry* 2:179–186.
26. Reissmann S (2007) Mechanism of action of group II chaperonins: impact of the built-in lid on the conformational cycle. (LMU München, Germany), Dissertation http://edoc.ub.uni-muenchen.de/7319/ p. 64.